



Since January 2020 Elsevier has created a COVID-19 resource centre with free information in English and Mandarin on the novel coronavirus COVID-19. The COVID-19 resource centre is hosted on Elsevier Connect, the company's public news and information website.

Elsevier hereby grants permission to make all its COVID-19-related research that is available on the COVID-19 resource centre - including this research content - immediately available in PubMed Central and other publicly funded repositories, such as the WHO COVID database with rights for unrestricted research re-use and analyses in any form or by any means with acknowledgement of the original source. These permissions are granted for free by Elsevier for as long as the COVID-19 resource centre remains active.



Clofazimine derivatives as potent broad-spectrum antiviral agents with dual-target mechanism



Xintong Zhang^{a,1}, Yulong Shi^{a,1}, Zhihao Guo^{a,1}, Xiaoqiang Zhao^a, Jiajing Wu^b, Shouchun Cao^b, Yonghua Liu^a, Yuhua Li^b, Weijin Huang^b, Youchun Wang^b, Qiang Liu^b, Yinghong Li^{a,**}, Danqing Song^{a,*}

^a Beijing Key Laboratory of Antimicrobial Agents, Institute of Medicinal Biotechnology, Peking Union Medical College and Chinese Academy of Medical Sciences, Beijing, 100050, China

^b National Institutes for Food and Drug Control, Beijing, 100050, China

ARTICLE INFO

Article history:

Received 22 December 2021

Received in revised form

6 February 2022

Accepted 17 February 2022

Available online 5 March 2022

Keywords:

Clofazimine analogues

Rabies virus

Structure–activity relationship

SARS-CoV-2

Broad-spectrum

ABSTRACT

Thirty-two clofazimine derivatives, of which twenty-two were new, were synthesized and evaluated for their antiviral effects against both rabies virus and pseudo-typed SARS-CoV-2, taking clofazimine (**1**) as the lead. Among them, compound **15f** bearing 4-methoxy-2-pyridyl at the N5-position showed superior or comparable antiviral activities to lead **1**, with the EC₅₀ values of 1.45 μM and 14.6 μM and the SI values of 223 and 6.1, respectively. Compound **15f** inhibited rabies and SARS-CoV-2 by targeting G or S protein to block membrane fusion, as well as binding to L protein or nsp13 to inhibit intracellular biosynthesis respectively, and thus synergistically exerted a broad-spectrum antiviral effect. The results provided useful scientific data for the development of clofazimine derivatives into a new class of broad-spectrum antiviral candidates.

© 2022 Elsevier Masson SAS. All rights reserved.

1. Introduction

Rabies virus, a negative-stranded RNA virus, causes fatal brain damage and other systematic symptoms, which leads to a mortality rate of nearly 100% [1–3]. To date, pre- or post-exposure prophylaxis, along with rabies immunoglobulin (RIG) is the only available way to protect the infected crowd [3]. However, multiple administrations of rabies vaccine and the public's lack of awareness hamper their in-time protection against the rabies virus [4–6], and an average of 60,000 people die from rabies each year globally [2]. The most favored Milwaukee protocol (M therapy) and its modified regimens obtained disappointing clinical outcomes [7,8]. Up to now, no drug has been approved for rabies treatment albeit with multiple efforts on drug discovery. Therefore, it is of great significance to find effective drugs for the treatment of rabies virus infection.

Recently, we found that riminophenazine alkaloid clofazimine (**1**, Fig. 1), an anti-leprosy and anti-tuberculous drug for clinical use, exhibited a good anti-rabies efficacy by affecting the g-glycoprotein (G protein)-mediated membrane fusion process [9]. At the meantime, Yuen's group discovered that it also effectively inhibits the replication of severe acute respiratory syndrome coronavirus 2 (SARS-CoV-2) both *in vitro* and *in vivo*, by interfering with spike glycoprotein (S protein)-mediated cell fusion and viral helicase activity [10]. These results indicated that **1** had a broad-spectrum antiviral activity, and deserved further investigation. However, highly lipophilic compound **1** upon therapeutic administration accumulates in lipid-rich tissues, and produces the most documented the red skin-coloring side effect [11], which might be alleviated by the reduction on lipophilicity [12,13].

Therefore, in the present study, taking **1** as the lead compound, several series of clofazimine analogues with reduced ClogP values were synthesized and evaluated for anti-rabies as well as anti-pseudo-typed SARS-CoV-2 (pSARS-CoV-2) activities. The anti-rabies structure–activity relationship (SAR) analysis, safety profile and the dual-target antiviral mechanism exploration of the key compound were presented.

* Corresponding author.

** Corresponding author.

E-mail addresses: liyinhong@imb.pumc.edu.cn (Y. Li), songdanqing@imb.pumc.edu.cn (D. Song).

¹ These authors made equal contributions to the work.

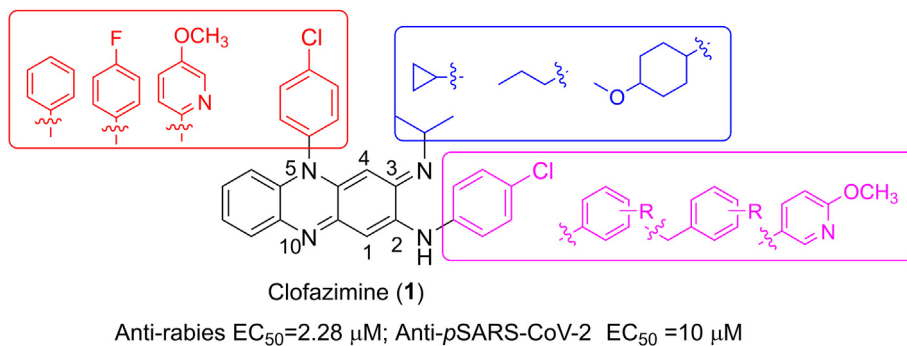
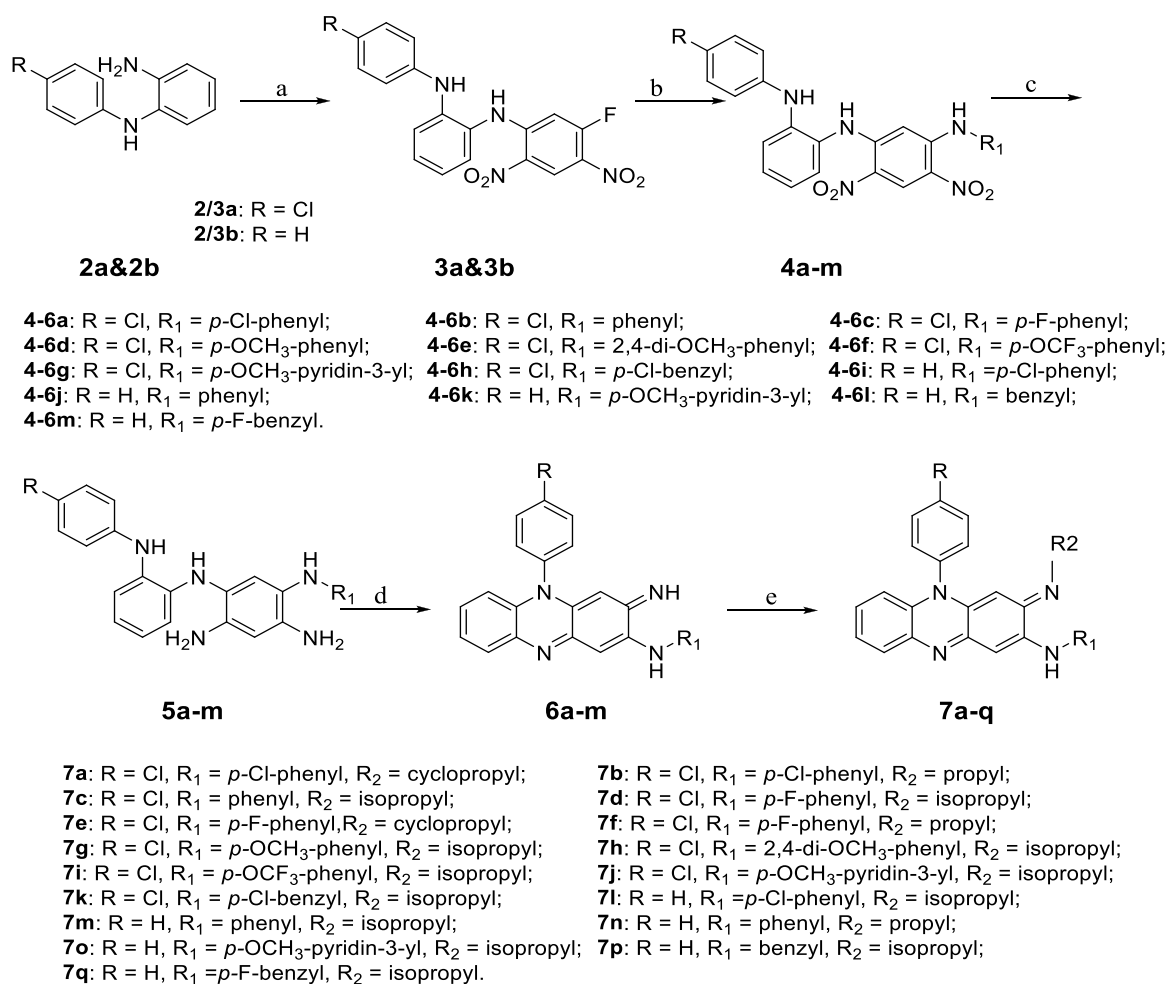


Fig. 1. The chemical structure, antiviral-activity and modification strategy of **1**.



Scheme 1. Reagents and conditions: (a) DFDNB, Et₃N, ethanol, rt; (b) Substituted aniline or benzylamine or 5-amino-2-methoxypyridine, Et₃N, THF, 64 °C; (c) Zn/acetic acid, ethanol, rt; (d) Air, ethanol, rt; (e) R₂NH₂, acetic acid, dioxane, 101 °C.

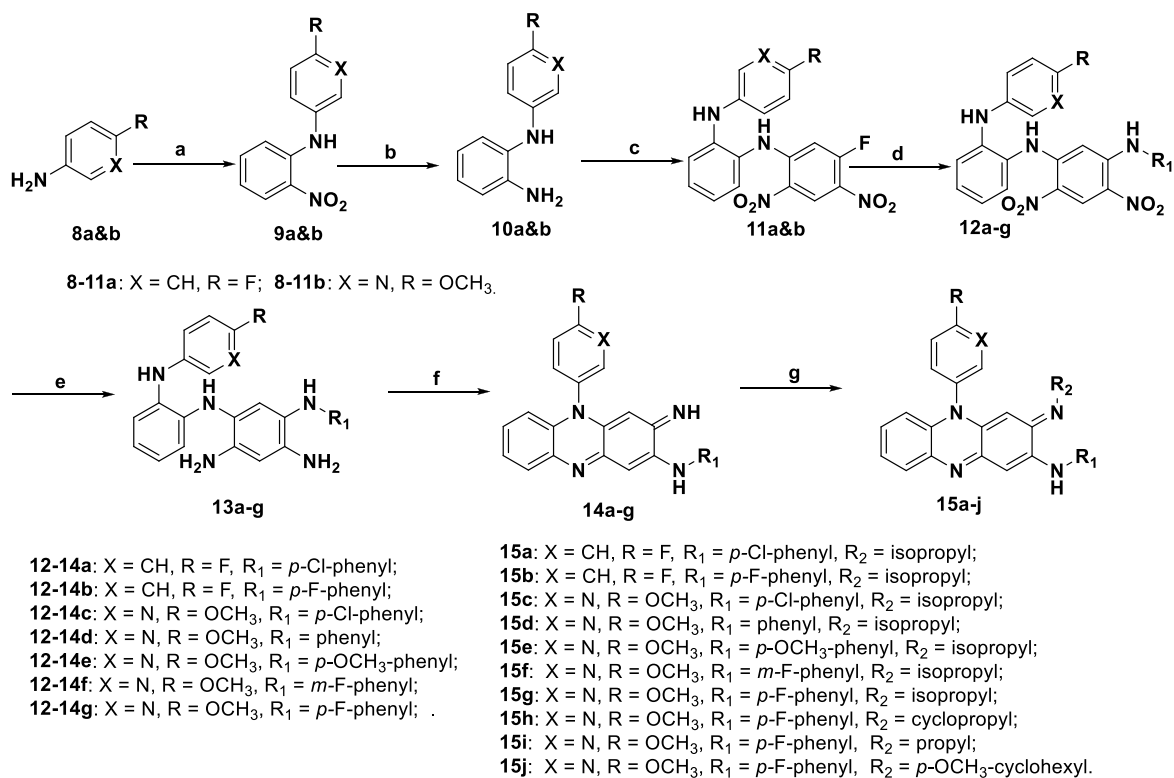
2. Result and discussion

2.1. Chemistry

A total of 32 clofazimine derivatives, of which 22 were new, were prepared as depicted in **Schemes 1 and 2** respectively. The synthesis of compounds **6a**, **6b**, **7a–c**, **7l–o** and **15b** were reported previously [13–19].

As shown in **Scheme 1**, nucleophilic substitution of starting material **2a** or **2b** with equimolar 1,5-difluoro-2,4-dinitrobenzene

(DFDNB) achieved **3a** or **3b**, which underwent a subsequent nucleophilic substitution reaction with various of amines, such as anilines, benzylamines or 5-amino-2-methoxypyridine, to give key intermediates **4a–m** in 78–95% yields. Reduction of nitro groups in **4a–m** by zinc powder in acetic acid and a subsequent oxidative cyclization under ambient condition achieved riminophenazines **6a–m** in yields of 24–55%. Finally, in the presence of acetic acid, the condensation of **6a–m** with varied amines led to target compounds **7a–q** in yields of 35–64%.



Scheme 2. Reagents and conditions: (a) 2-Fluoronitrobenzene, Et₃N or NaHCO₃, DMF, 90–100 °C; (b) 10% Pd/C, H₂, ethanol, rt; (c) DFDNB, Et₃N, ethanol, rt; (d) R₁NH₂, Et₃N, THF, 64 °C; (e) 10% Pd/C, H₂, methanol/THF, rt; (f) Air, ethanol/CH₂Cl₂, rt; (g) R₂NH₂, acetic acid, dioxane, 101 °C.

As described in Scheme 2, the nucleophilic substitution between **8a** or **8b** at 90–100 °C in DMF achieved **9a** or **9b** in yields of 55–61% instead of the conventional fusing reaction operation [13], followed by a reduction via Pd–C hydrogenation to yield key intermediate **10a** or **10b** in good yields. Next, following a similar five-step procedure as shown in Scheme 1, including nucleophilic substitution with DFDNB, nitro reduction, nucleophilic substitution with varied anilines, nitro reduction via Pd–C hydrogenation and ambient oxidation, compounds **14a–g** were gained in yields of 46–80%. Finally, products **15a–j** were acquired via condensation of compounds **14a–g** with amines in the presence of acetic acid in yields of 48–80%. The products were isolated for the flash column chromatography with petroleum ether/CH₂Cl₂ or CH₂Cl₂/ethyl acetate as eluent.

2.2. SAR for anti-rabies activity of the target compounds in BSR cells

All target compounds were measured for their *in vitro* anti-rabies activities in BSR cells using rapid fluorescent focus inhibition test (RFFIT) assay constructed in our lab, taking **1** as the control [9]. The combination of the EC₅₀ and selectivity index (SI, CC₅₀/EC₅₀ ratio) values of each compound was taken as the evaluation reference for antiviral potency. The structures and anti-rabies activities of all the target compounds were listed in Table 1.

Initially, different substituents were introduced on the imine N atom at C-3 position to generate compounds **6a** (H), **7a** (cyclopropyl) and **7b** (*n*-propyl), and their anti-rabies activity displayed declined activity. It was speculated that isopropyl group on the imine N atom might be beneficial for activity.

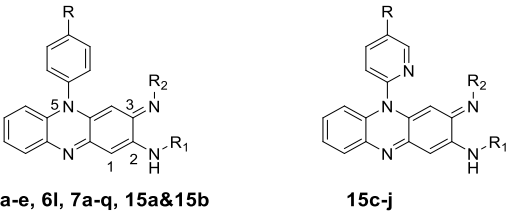
Next, the 3-isopropyl imine was retained, and the *p*-chloroaniline moiety attached on C-2 position was replaced by different anilines, 6-methoxy-3-pyridylamine or phenylethylamine, to

generate compounds **7c**, **7d** and **7g–k**. Most of them gave decreased activity to varying degrees, except that compounds **7i** with *p*-trifluoromethoxyaniline and **7k** with *p*-chlorobenzylamine displayed comparable activities to the lead **1**, with the IC₅₀ values of 1.77 μM and 0.76 μM and SI values of 182 and 123, respectively. Then, the 3-isopropyl imine was kept, modification on the N-5 substituents was carried out, and *p*-chlorophenyl moiety was altered into phenyl, *p*-fluorophenyl or 6-methoxy-3-pyridylamine, and the corresponding analogues **7l**, **7m**, **7o–q** and **15a–g** were generated and evaluated. Among them, compounds **7l**, **7p** and **7q** bearing a *p*-chloroaniline, benzylamine and *p*-fluorobenzylamine on their C-2 position gave elevated antiviral activity with the IC₅₀ values of 1.40, 1.40 and 1.90 μM respectively, as well as obviously increased cytotoxicity. Compounds **15f** and **15g** displayed the highest antiviral activity, with IC₅₀ value of 1.45 μM and 1.41 μM, and SI value of 223 and 229, respectively. Meanwhile, the replacement of 3-isopropyl imine with imine, cyclopropyl imine, propyl imine or 4-methoxycyclohexyl imine led to decreased activity as in all cases of compounds **6b**, **6d**, **6e**, **6l**, **7e**, **7f**, **7n** and **15h–j**, and 3-isopropyl imine was thus considered as a beneficial moiety for the anti-rabies activity.

2.3. The anti-pSARS-CoV-2 activity of the target compounds in Huh7 cells

Meanwhile, the anti-SARS-CoV-2 activities of target clofazimine derivatives were evaluated on an S protein-based pSARS-CoV-2 model in Huh 7 cells constructed in our lab [20,21], taking **1** as the positive control. As indicated in Table 2, the anti-pSARS-CoV-2 activity tendency of most compounds was similar to the anti-rabies tendency as disclosed above, and compounds **7m**, **15f** and **15g** gave elevated activities compared to **1**. Especially, compounds **15f**

Table 1
Anti-rabies activity and cytotoxicity of all the target compounds.



	R	R ₁	R ₂	CC ₅₀ (μM) ^a	EC ₅₀ (μM) ^b	SI ^c	ClogP ^d
1	Cl			323	2.28	141	5.39
6a	Cl		H	35.4	20.6	1.7	4.50
6b	Cl		H	35.4	20.6	1.7	3.94
6d	Cl		H	106	106	1.0	3.82
6e	Cl		H	35.4	35.4	1.0	3.69
6l	H		H	35.4	35.4	1.0	4.71
7a	Cl			323	22.7	14.2	5.03
7b	Cl			323	24.9	13.0	5.56
7c	Cl			185	8.44	21.9	4.83
7d	Cl			281	4.56	61.7	4.99
7e	Cl			323	6.86	47.1	4.63
7f	Cl			54.5	1.67	32.6	5.16
7g	Cl			130	6.86	19.0	4.71
7h	Cl			120	6.86	17.6	4.58
7i	Cl			323	1.77	182	6.36
7j	Cl			35.4	2.29	15.5	4.09
7k	Cl			93.1	0.76	123	5.60
7l	H			42.6	1.90	22.4	4.83
7m	H			323	10.7	30.1	4.28
7n	H			14.4	0.76	19.0	4.44
7o	H			107	5.03	21.2	3.53
7p	H			107	1.40	76.4	4.49
7q	H			17.3	1.90	9.1	4.64
15a	F			223	4.02	55.6	4.99
15b	F			314	2.29	134	4.59

Table 1 (continued)

	R	R ₁	R ₂	CC ₅₀ (μM) ^a	EC ₅₀ (μM) ^b	SI ^c	ClogP ^d
15c	OCH ₃			107	5.03	21.3	4.09
15d	OCH ₃			323	12.3	26.3	3.53
15e	OCH ₃			323	13.2	24.5	3.40
15f	OCH ₃			323	1.45	223	3.69
15g	OCH ₃			323	1.41	229	3.69
15h	OCH ₃			107	13.2	8.1	3.33
15i	OCH ₃			107	1.40	76.4	3.86
15j	OCH ₃			84.4	2.55	33.1	3.71

^a Cytotoxic concentration required to inhibit BSR cell growth by 50%.

^b Concentration required to inhibit rabies virus growth by 50%.

^c Selectivity Index values equaled to CC₅₀/EC₅₀.

^d Calculated by Chemdraw 14.0 (CambridgeSoft).

Table 2
Anti-pSARS-CoV-2 activity and cytotoxicity of all the target compounds.

Code	pSARS-CoV-2			Code	pSARS-CoV-2		
	CC ₅₀ (μM) ^a	EC ₅₀ (μM) ^b	SI ^c		CC ₅₀ (μM) ^a	EC ₅₀ (μM) ^b	SI ^c
1	44.7	10	4.5	7l	16.1	<10	>1.6
6a	NT ^d	NT	NT	7m	177	17.2	10.2
6b	<10	<10	/	7n	35.6	<10	>3.5
6d	>267	154	>1.7	7o	22.7	13.5	1.7
6e	16.6	16.1	1.0	7p	<10	<10	/
6l	NT	NT	NT	7q	29.6	<10	>2.9
7a	>267	141	>1.9	15a	17.0	29.6	0.6
7b	107	39.3	2.7	15b	267	81.1	3.3
7c	154	40.9	3.8	15c	51.3	<10	>5.1
7d	40.6	14.5	2.8	15d	<10	<10	/
7e	16.7	13.5	1.2	15e	17.1	<10	>1.7
7f	14.9	10.3	1.5	15f	88.9	14.6	6.1
7g	88.9	16.6	5.4	15g	88.9	<10	>8.9
7h	13.52	<10	>1.3	15h	88.9	33.1	2.7
7i	38.37	9.98	3.8	15i	<10	<10	/
7j	>267	153	>1.7	15j	51.3	<10	>5.1
7k	16.1	12.4	1.3				

^a Cytotoxic concentration required to inhibit Huh 7 cell growth by 50%.

^b Concentration required to reduce 50% of the virus level in Huh 7 cell.

^c Selectivity Index values equaled to CC₅₀/EC₅₀.

^d NT: not tested.

and **15g** gave the EC₅₀ values of 14.6 μM and <10 μM, and SI values of 6.1 and >8.9, respectively, suggesting that **15f** and **15g** might own a broad-spectrum antiviral activity against rabies viruses and pSARS-Cov-2, worthy of the further investigation.

2.4. The safety profiles of compounds **15g** and **15f**

To evaluate the safety profiles of **15g** and **15f**, an acute toxicity test was performed in Kunming mice. Both compounds were given orally in a single-dosing experiment at 0, 200, 400, 600 and 800 mg•kg⁻¹, respectively. The mice were closely monitored for 7 days, and all the surviving mice had glossy hair, fleshy body and good appetite. Therefore, the median lethal dose (LD₅₀) value for both **15g** and **15f** was over 800 mg•kg⁻¹, indicating their good safety profiles *in vivo*.

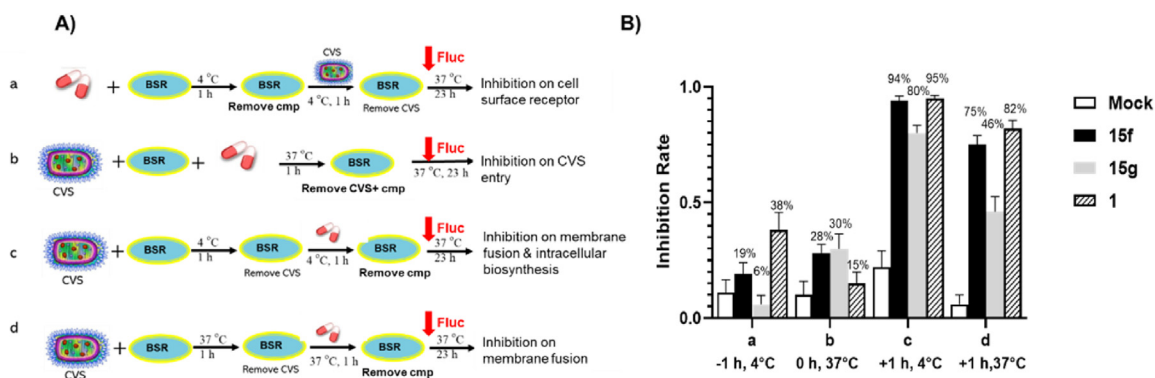


Fig. 2. A single-cycle time-of-addition experiment was conducted with rabies CVS strain. A) Compound **15f**, **15g** or **1** (25 μ M) was added and left for 1 h before infection (-1 h), during infection (0 h), and for 1 h after infection ($+1$ h). After incubated for 23 h, inhibition of rabies infection was detected as a decrease in luciferase signal. B) Inhibition of rabies CVS infection by a test compound was detected as a decrease in fluorescence activity, and error bars indicate standard deviations. The experiment was repeated for 3 times.

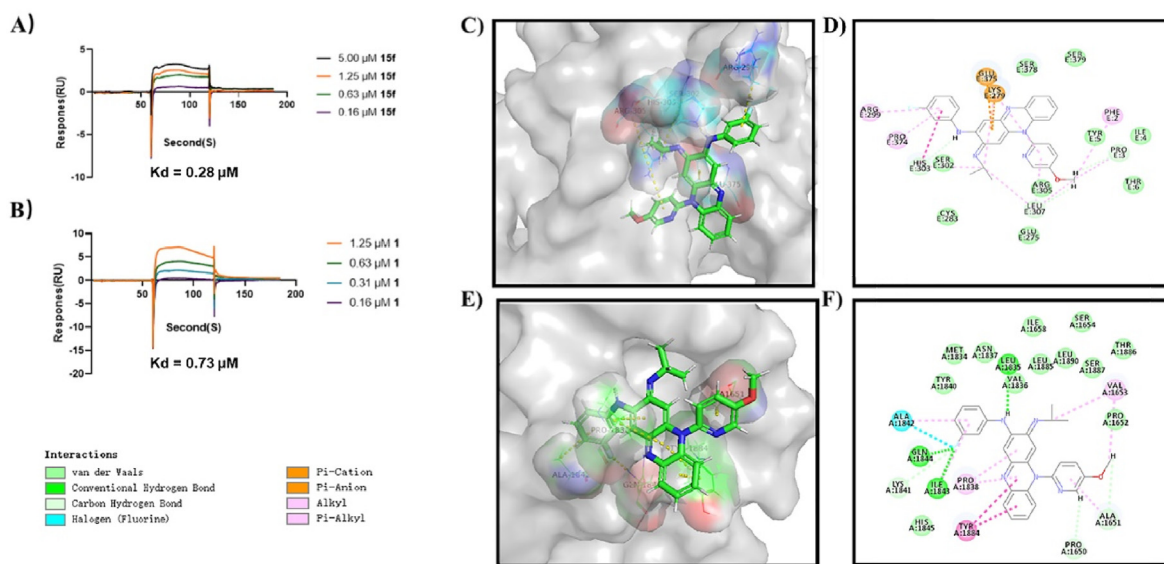


Fig. 3. A, B) SPR sensorgrams obtained on a rabies virus glycoprotein-coated chip at different concentrations of **15f** and **1**. C–F) Molecular docking models of **15f** bound to rabies virus glycoprotein (PDB ID: 6LGW) or rabies L protein (PDB ID: 6EUB) by Discovery Studio 4.5. C, E) Solid surface map of the interaction pockets with compound **15f**. D, F) 2D modes of interaction pockets with compound **15f**. Ligand is colored by element type (N, blue; O, red; F, light blue), key bonds are indicated by dashed lines between the atoms involved, and the colors of key bonds and residues are shown according to the interaction mode.

2.5. Mechanism of action of the key compounds

2.5.1. Time of addition assay

In order to figure out the precise step of rabies proliferation that is blocked by the key compounds, we first evaluated their anti-rabies activity using a time-of-addition assay in a single infectious cycle in BSR cells. As illustrated in Fig. 2A, compounds **15f** or **15g** was incubated into BSR cells at 1 h before rabies challenge virus standard (CVS) strain infection (-1 h), during infection (0 h), or 1 h post infection ($+1$ h), taking compound **1** as the positive control and DMSO as a negative control. As shown in Fig. 2B, both compounds **15f** and **15g** exerted strong inhibitory effects when added 1 h post infection at both 4 $^{\circ}$ C and 37 $^{\circ}$ C, indicating that they interfered with the viral membrane fusion and intracellular biosynthesis, similar to the lead **1**. The results suggested that they might have dual-target or multi-target mechanism against rabies virus, and the inhibitory behavior of compound **15f** was highly similar to that of the lead **1**.

2.5.2. Dual-target mechanism of compound **15f** against rabies virus

Our earlier molecular docking analysis indicated that compound **1** might target rabies G protein to interfere with viral membrane fusion [9], therefore, the recombinant rabies G protein was prepared, and surface plasmon resonance (SPR) assay was conducted to further confirm the direct interaction between rabies G protein and compound **15f**. As depicted in Fig. 3A and B, it displayed the concentration-dependent binding with immobilized G protein with K_d value of 0.28 μ M, while **1** gave the K_d value of 0.73 μ M. Then, molecular docking analysis between rabies G protein (PDB ID: 6LGW) and **15f** was performed by Discovery Studio 4.5. As disclosed in Fig. 3C and D, van der waals force and hydrophobic interactions contributed to the strong interaction between **15f** and G protein, and gave the Libdock scores of 106.1. These results demonstrated that compound **15f** blocked rabies viral membrane fusion by binding to G protein.

Among all 5 proteins expressed by rabies RNA genome, L protein plays the vital role in conducting the RdRp activity in rabies virus [22]. Therefore, molecular docking analysis between compound **15f**

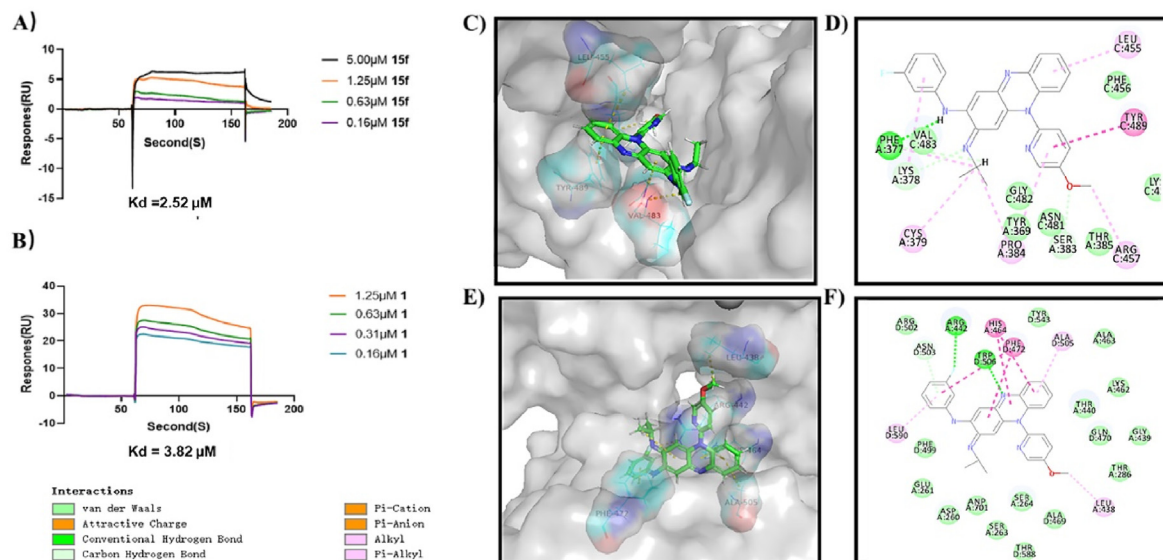


Fig. 4. A, B) SPR sensorgrams obtained on a SARS-CoV-2 S protein-coated chip at different concentrations of **15f** and **1**. C–F) Molecular docking models of **15f** bound to SARS-CoV-2 S protein (PDB ID: 6VSB) or nsp13 (PDB ID: 7NNO) by Discovery Studio 4.5. C, E) Solid surface map of the interaction pockets with compound **15f**. D, F) 2D modes of interaction pockets with compound **15f**. Ligand is colored by element type (N, blue; O, red; F, light blue), key bonds are indicated by dashed lines between the atoms involved, and the colors of key bonds and residues are shown according to the interaction mode.

with lyssavirus L protein (PDB ID: 6EUB) was launched by Discovery Studio 4.5, taking **1** as the control. It gave a high Libdock score of 106.7, while **1** gave that of 104.7. As disclosed in Fig. 3E and F and Supplementary Figs. S1A and S1B, the multiple hydrogen bonds with Leu1835, Ile1843 and Gln1844 between **15f** and L protein might contribute to the higher affinity of **15f** over **1**, suggesting that compound **15f** might directly bind to rabies L protein, and thus inhibit the viral biosynthesis. Our results indicated that compound **15f** might exert the anti-rabies efficiency by simultaneously targeting G protein and L protein in the membrane fusion and intracellular biosynthesis stages respectively, consistent with the above time-of-addition results.

2.5.3. Dual-target mechanism of compound **15f** against SARS-CoV-2

Similarly, the direct interaction between recombinant SARS-CoV-2 S protein and **15f** was conducted by SPR assay, taking **1** as the control. As demonstrated in Fig. 4A and B, compound **15f** could directly bind to immobilized SARS-CoV-2 S protein in a concentration-dependent manner, and gave the Kd value of 2.52 μM , while **1** gave the that of 3.82 μM . The molecular docking analysis between compound **15f** and SARS-CoV-2 S protein (PDB ID: 6VSB) was performed (Fig. 4C and D), taking **1** as the control (Supplementary Figs. S1C and S1D). Compound **15f** gave the Libdock scores of 124.1, while lead **1** gave the score of 118.6. As disclosed in Fig. 4C and D, besides the hydrogen bond between their N2 atoms with Phe377 and Val483 respectively, they fit in a T-shaped cavity of SARS-CoV-2 S protein, which was accomplished by the planar tricyclic scaffold and the pyridine or benzene moiety respectively. And the residues Thr385, Lys458, Arg547 and Ser383 might mainly contribute to strong van der Waals force between **15f** and the target S protein.

Since lead **1** inhibited the unwinding activity of nsp13 in the SARS-CoV-2 viral biosynthesis [10], the direct interaction between nsp13 (PDB ID: 7NNO) and compound **15f** was predicted by docking analysis (Fig. 4E and F), taking **1** as the control (Supplementary Figs. S1E and S1F). Compounds **15f** and **1** gave reasonable Libdock scores of 110.0 and 103.0, respectively. Apparently, they fit well in the same cavity, and formed a common hydrogen bond between the N10 atom and Trp506, but compound **15f** also formed a second

hydrogen bond between fluorine atom and Arg272, which might contribute to its higher affinity. Besides, both of them formed π - π stacking effect with His464 and Phe472, indicating that **15f** might directly target nsp13 to inhibit SARS-CoV-2 biosynthesis.

As shown in Fig. 5, our results suggested that clofazimine derivative **15f** might simultaneously bind to the rabies G protein in viral membrane fusion, as well as L protein in viral biosynthesis stage, and synergistically exert the anti-rabies activity. Similarly, it could also simultaneously target SARS-CoV-2 S protein in viral membrane fusion, and nsp13 in viral biosynthesis to inhibit the proliferation of SARS-CoV-2, and thus shed light on the discovery of a new class of broad-spectrum antiviral agent through a dual-target mechanism.

3. Conclusions

To sum up, 32 clofazimine derivatives, of which 22 were new, were designed, synthesized and evaluated for their antiviral activity against rabies and pSARS-CoV-2 viruses, taking **1** as the lead. Compound **15f** showed potent antiviral activities with the IC₅₀ values of 1.45 μM and 14.6 μM and the SI values of 223 and 6.1, respectively, superior or comparable to those of lead **1**. Additionally, it gave a good safety profile with the oral LD₅₀ value of over 800 $\text{mg}\cdot\text{kg}^{-1}$. Compound **15f** affected the rabies and SARS-CoV-2 proliferation by targeting G or S protein to block the viral membrane fusion, as well as binding to L protein or nsp13 to inhibit viral biosynthesis, respectively, and thus synergistically exerted antiviral effect. And our study provided useful scientific data for the development of clofazimine derivatives as a new class of broad-spectrum antiviral candidates with a dual-target antiviral mechanism, worthy of further investigation.

4. Experimental section

4.1. Chemistry

4.1.1. General

All commercial reagents and solvents were obtained from the commercial provider and used without further purification.

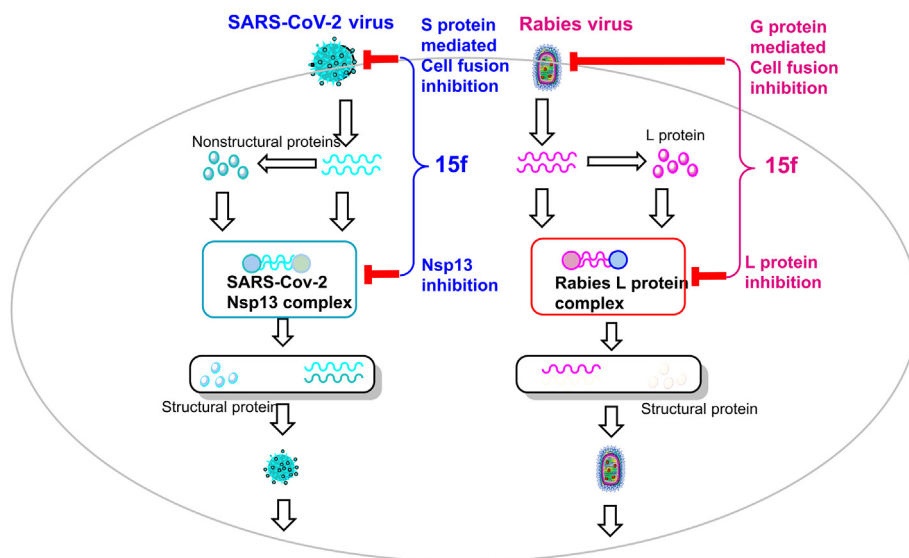


Fig. 5. The dual-target mechanism of compound **15f** against rabies and SARS-CoV-2.

Melting points (mp) were obtained with a MP90 melting point apparatus (Mettler-Toledo, Greifensee, Switzerland). ^1H NMR and ^{13}C NMR spectra were recorded on a Bruker Avance III 500 or II600 spectrometers (Varian, San Francisco, USA) in $\text{DMSO-}d_6$ with Me_4Si as the internal standard. ESI high-resolution mass spectra (HRMS) were recorded on an Autospec Ultima-TOF spectrometer (Micro-mass UK Ltd., Manchester, U.K.). Flash chromatography over silica gel was performed on Combiflash Rf 200 (Teledyne, Nebraska, USA). Compounds **6a**, **6b**, **7a–c**, **7l–o** and **15b** were synthesized and identified by mp or ^1H NMR [13–19].

4.1.2. General procedures for synthesis of compounds **6a–h**

To a solution of refined *N*-(4-chlorophenyl)-1,2-benzenediamone (**2a**, 45.9 mmol) in ethanol (120 mL), DFDNB (1.1 equiv) and TEA (1.1 equiv) were added successively, and the mixture was stirred at rt for 3 h. The formed precipitate was filtered, and the solid was washed with water (50 mL \times 2) and ethanol (60 mL \times 2) successively to give the intermediate **3a** as an orange solid in a 97% yield. To a solution of **3a** (2.5 mmol) in THF (16 mL), TEA (1 equiv.) and substituted aniline (1.1 equiv) were added. The reaction mixture was warmed to 60–70 °C and stirred overnight. The solvent was removed *in vacuo*, and the residue was slurried with ethanol (20 mL). The formed suspension was filtered, and the solid was washed with water and ethanol to give **4a–h** as orange solid in yields of 73–93%.

To a suspension of **4a–h** (2.0 mmol) in ethanol (20 mL) and acetic acid (6 mL), zinc powder (30 equiv) was added portionwise. The mixture was stirred at rt until the color turned to light green, filtered, and washed with ethanol and DCM. The filtrate was concentrated, water was added to the residue and made alkaline by ammonia. The formed precipitate was filtered and washed with water to gain the intermediates **5a–h**, which was suspended or dissolved in ethanol (20 mL) and then was stirred under air overnight. The precipitation was filtered to give **6a–h**, which was purified by flash chromatography using a gradient of $\text{CH}_2\text{Cl}_2/\text{CH}_3\text{OH}$ as the eluent.

4.1.2.1. 2-*p*-Methoxyanilino-3-imino-5-*p*-chlorophenyl-3,5-dihydrophenazine (6d**).** Yield: 48%; red solid; mp: 217–219 °C; ^1H NMR (500 MHz, CDCl_3) δ 7.72–7.69 (3H, m, Ar–H), 7.31–7.29 (2H, m, Ar–H), 7.29–7.27 (2H, m, Ar–H), 7.22–7.18 (1H, m, Ar–H),

7.18–7.13 (1H, m, Ar–H), 6.95–6.92 (2H, m, Ar–H), 6.75 (1H, s, 1-H), 6.50 (1H, d, $J = 8.2$ Hz, Ar–H), 5.19 (1H, s, 4-H) 3.83 (3H, s, OMe); ^{13}C NMR (126 MHz, CDCl_3) δ 161.4, 156.6, 150.8, 145.0, 135.9, 135.8, 135.5, 134.0, 132.3, 131.7 (2), 130.9, 130.4 (2), 128.3, 127.7, 124.6 (2), 123.1, 114.7 (2), 114.0, 98.8, 96.8, 55.6; HRMS: calcd for $\text{C}_{25}\text{H}_{20}\text{ClON}_4$ $[\text{M}+\text{H}]^+$ 427.1320, found: 427.1318.

4.1.2.2. 2-(2,4-Dimethoxyanilino)-3-imino-5-*p*-chlorophenyl-3,5-dihydrophenazine (6e**).** Yield: 35%; red solid; mp: 186–188 °C; ^1H NMR (500 MHz, CDCl_3) δ 8.37–8.18 (2H, m, NH), 7.72–7.66 (3H, m, Ar–H), 7.50 (1H, d, $J = 8.6$ Hz, Ar–H), 7.30–7.26 (2H, m, Ar–H), 7.20–7.16 (1H, m, Ar–H), 7.15–7.11 (1H, m, Ar–H), 6.81 (1H, s, 1-H), 6.55–6.53 (1H, m, Ar–H), 6.53–6.50 (1H, m, Ar–H), 6.49–6.46 (1H, m, Ar–H), 5.16 (1H, s, 4-H), 3.84 (3H, s, OMe), 3.83 (3H, s, OMe); ^{13}C NMR (126 MHz, CDCl_3) δ 161.7, 156.9, 152.7, 151.0, 144.1, 135.9, 135.7, 135.5, 133.9, 131.6 (2), 131.0, 130.4 (2), 128.2, 127.5, 123.0, 122.4, 122.1, 113.9, 103.7, 99.4, 98.9, 97.1, 55.7, 55.6; HRMS: calcd for $\text{C}_{26}\text{H}_{22}\text{O}_2\text{ClN}_4$ $[\text{M}+\text{H}]^+$ 457.1426, found: 457.1426.

4.1.3. General procedures for synthesis of compounds **6i–m**

The title compound was prepared following a similar procedure in 4.1.2, taking 2-aminodiphenylamine (**2b**) as the starting material.

4.1.3.1. 2-Benzyl-3-imino-5-phenyl-3,5-dihydrophenazine (6l**).** Yield: 36%; red solid; mp: 186–188 °C; ^1H NMR (500 MHz, $\text{DMSO-}d_6$) δ 9.28 (1H, br s, NH), 7.78–7.73 (2H, m, Ar–H), 7.69–7.65 (1H, m, Ar–H), 7.56–7.53 (1H, m, Ar–H), 7.45–7.42 (2H, m, Ar–H), 7.39–7.33 (5H, m, Ar–H), 7.28–7.23 (1H, m, Ar–H), 7.14–7.10 (2H, m, Ar–H), 6.34–6.30 (1H, m, NH), 5.95 (1H, s, 1-H), 5.17 (1H, s, 4-H), 4.51 (2H, d, $J = 5.4$ Hz, CH_2Ar); ^{13}C NMR (126 MHz, $\text{DMSO-}d_6$) δ 159.7, 150.2, 147.3, 138.7, 137.1, 134.8, 132.9, 131.2 (2), 130.9, 129.6, 128.7(2), 128.4 (2), 127.1, 126.9 (3), 126.8, 122.1, 113.7, 96.4, 96.3, 45.4; HRMS: calcd for $\text{C}_{25}\text{H}_{21}\text{N}_4$ $[\text{M}+\text{H}]^+$ 377.1761, found: 377.1760.

4.1.4. General procedures for synthesis of compounds **7d–k**, **7o** and **7p**

To a suspension of **6a–m** (0.24 mmol) in dioxane (3 mL), acetic acid (2 drops) and different amine (10 or 20 equiv) were added, and then the reaction mixture stirred at 101 °C for 5 h before evaporation *in vacuo*. The residue was partitioned between CH_2Cl_2 (20 mL) and water (20 mL), then the water phase was extracted

with CH_2Cl_2 (20 mL). The combined organic phases were washed with water (30 mL x 3) and brine (40 mL) successively, dried over anhydrous Na_2SO_4 , filtered and evaporated. The residue was purified over by flash chromatography using a gradient of petroleum ether/ CH_2Cl_2 as the eluent, and gave the title compounds.

4.1.4.1. 2-p-Fluoroanilino-3-isopropylimino-5-p-chlorophenyl-3,5-dihydrophenazine (7d). Yield: 57%; red solid; mp: 210–212 °C; ^1H NMR (400 MHz, CDCl_3) δ 7.73–7.65 (3H, m, Ar–H), 7.34–7.28 (4H, m, Ar–H), 7.18–7.09 (2H, m, Ar–H), 7.09–7.04 (2H, m, Ar–H), 6.71 (1H, s, 1-CH), 6.44 (1H, d, J = 7.9 Hz, Ar–H), 5.27 (1H, s, 4-CH), 3.52–3.42 (1H, m, CHMe_2), 1.09 (6H, d, J = 6.2 Hz, CHMe_2); ^{13}C NMR (101 MHz, CDCl_3) δ 160.4, 158.0, 151.2, 150.5, 144.8, 136.2, 135.9, 135.6, 134.8, 131.7 (2), 131.4, 130.5 (2), 128.1, 127.3, 124.2, 124.1, 122.9, 116.1, 115.9, 113.8, 98.2, 89.1, 49.4, 23.6 (2); HRMS: calcd for $\text{C}_{27}\text{H}_{23}\text{N}_4\text{ClF}$ $[\text{M}+\text{H}]^+$ 457.1590, found: 457.1589.

4.1.4.2. 2-p-Fluoroanilino-3-cyclopropylimino-5-p-chlorophenyl-3,5-dihydrophenazine (7e). Yield: 55%; red solid; mp: 215–217 °C; ^1H NMR (400 MHz, CDCl_3) δ 7.72–7.67 (2H, m, Ar–H), 7.67–7.63 (1H, m, Ar–H), 7.35–7.30 (2H, m, Ar–H), 7.30–7.26 (2H, m, Ar–H), 7.18–7.03 (4H, m, Ar–H), 6.65 (1H, s, 1-H), 6.44–6.40 (1H, m, Ar–H), 5.54 (1H, s, 4-H), 2.79–2.71 (1H, m, CHCH_2CH_2), 0.92–0.76 (4H, m, CHCH_2CH_2); ^{13}C NMR (101 MHz, CDCl_3) δ 159.3 (d, J = 242.0 Hz, 1C–F), 152.5, 151.4, 144.6, 136.2, 135.8, 135.6, 134.6, 131.7 (3), 131.5, 130.6 (2), 128.1, 127.3, 124.4, 124.3, 122.9, 116.1 (2) (d, J = 23.0 Hz, 2C–F), 113.8, 98.2, 89.4, 32.9, 10.0 (2); HRMS: calcd for $\text{C}_{27}\text{H}_{21}\text{N}_4\text{ClF}$ $[\text{M}+\text{H}]^+$ 455.1433, found: 455.1433.

4.1.4.3. 2-p-Fluoroanilino-3-propylimino-5-p-chlorophenyl-3,5-dihydrophenazine (7f). Yield: 56%; red solid; mp: 176–178 °C; ^1H NMR (400 MHz, CDCl_3) δ 7.73–7.67 (3H, m, Ar–H), 7.33–7.28 (4H, m, Ar–H), 7.20–7.11 (2H, m, Ar–H), 7.10–7.04 (2H, m, Ar–H), 6.72 (1H, s, 1-H), 6.45 (1H, d, J = 7.7 Hz, Ar–H), 5.27 (1H, s, 4-H), 3.11 (2H, t, J = 6.8 Hz, $\text{CH}_2\text{CH}_2\text{CH}_3$), 1.72–1.63 (2H, m, $\text{CH}_2\text{CH}_2\text{CH}_3$), 0.94 (3H, t, J = 7.4 Hz, $\text{CH}_2\text{CH}_2\text{CH}_3$); ^{13}C NMR (101 MHz, CDCl_3) δ 159.3 (d, J = 242.0 Hz, 1C–F), 152.4, 151.2, 144.7, 136.1, 135.8, 135.7, 134.7, 131.7 (3), 131.3, 130.4 (2), 128.2, 127.4, 124.3, 124.2, 123.0, 116.1 (2) (d, J = 23.0 Hz, 2C–F), 113.9, 98.1, 89.1, 52.0, 24.3, 12.3; HRMS: calcd for $\text{C}_{27}\text{H}_{23}\text{N}_4\text{ClF}$ $[\text{M}+\text{H}]^+$ 457.1590, found: 457.1590.

4.1.4.4. 2-p-Methoxyanilino-3-isopropylimino-5-p-chlorophenyl-3,5-dihydrophenazine (7g). Yield: 54%; red solid; mp: 178–180 °C; ^1H NMR (500 MHz, CDCl_3) δ 7.73–7.68 (2H, m, Ar–H), 7.65 (1H, d, J = 7.7 Hz, Ar–H), 7.31–7.27 (4H, m, Ar–H), 7.15 (1H, m, Ar–H), 7.09 (1H, m, Ar–H), 6.94–6.89 (2H, m, Ar–H), 6.66 (1H, s, 1-H), 6.43 (1H, d, J = 8.1 Hz, Ar–H), 5.27 (1H, s, 4-H), 3.83 (3H, s, OMe), 3.50–3.43 (1H, m, CHMe_2), 1.09 (6H, d, J = 6.2 Hz, CHMe_2); ^{13}C NMR (126 MHz, CDCl_3) δ 156.3, 151.2, 150.6, 145.5, 136.2, 135.7, 135.5, 134.7, 132.7, 131.6 (2), 131.3, 130.5 (2), 127.9, 126.9, 124.5 (2), 122.8, 114.5 (2), 113.8, 97.5, 89.0, 55.6, 49.3, 23.6 (2); HRMS: calcd for $\text{C}_{28}\text{H}_{26}\text{ON}_4\text{Cl}$ $[\text{M}+\text{H}]^+$ 469.1790, found: 469.1791.

4.1.4.5. 2-(2,4-Dimethoxyanilino)-3-isopropylimino-5-p-chlorophenyl-3,5-dihydrophenazine (7h). Yield: 46%; red solid; mp: 190–192 °C; ^1H NMR (500 MHz, CDCl_3) δ 7.72–7.67 (2H, m, Ar–H), 7.65 (1H, d, J = 8.0 Hz, Ar–H), 7.46 (1H, m, Ar–H), 7.31–7.27 (2H, m, Ar–H), 7.17–7.11 (1H, m, Ar–H), 7.11–7.05 (1H, m, Ar–H), 6.69 (1H, s, 1-H), 6.53 (1H, s, Ar–H), 6.50 (1H, d, J = 8.5 Hz, Ar–H), 6.42 (1H, d, J = 7.7 Hz, Ar–H), 5.27 (1H, s, 4-H), 3.83 (6H, s, OMe, OMe), 3.52–3.43 (1H, m, CHMe_2), 1.10 (6H, d, J = 6.2 Hz, CHMe_2); ^{13}C NMR (101 MHz, CDCl_3) δ 156.9, 153.1, 151.6, 151.0, 145.1, 136.5, 135.9, 135.6, 134.8, 131.7 (2), 130.7 (2), 128.0, 126.9, 123.0, 122.8, 122.7,

113.9, 110.1, 104.0, 99.6, 98.0, 89.4, 56.0, 55.8, 49.5, 23.7 (2); HRMS: calcd for $\text{C}_{29}\text{H}_{28}\text{O}_2\text{N}_4\text{Cl}$ $[\text{M}+\text{H}]^+$ 499.1895, found: 499.1892.

4.1.4.6. 2-p-Trifluoromethoxyanilino-3-isopropylimino-5-p-chlorophenyl-3,5-dihydrophenazine (7i). Yield: 63%; red solid; mp: 200–202 °C; ^1H NMR (400 MHz, CDCl_3) δ 7.73–7.67 (3H, m, Ar–H), 7.39–7.34 (2H, m, Ar–H), 7.32–7.27 (2H, m, Ar–H), 7.24–7.19 (2H, m, Ar–H), 7.19–7.09 (2H, m, Ar–H), 6.82 (1H, s, 1-H), 6.46–6.42 (1H, m, Ar–H), 5.28 (1H, s, 4-H), 3.51–3.41 (1H, m, CHMe_2), 1.09 (6H, d, J = 6.2 Hz, CHMe_2); ^{13}C NMR (101 MHz, CDCl_3) δ 151.1, 150.4, 144.7 (2), 144.0, 138.8, 136.1, 135.7, 135.6, 134.8, 131.7 (2), 131.5, 130.5 (2), 128.2, 127.6, 123.0, 122.9 (2), 122.2 (2), 113.9, 99.0, 89.1, 49.4, 23.6 (2); HRMS: calcd for $\text{C}_{28}\text{H}_{23}\text{ON}_4\text{ClF}_3$ $[\text{M}+\text{H}]^+$ 523.1507, found: 523.1509.

4.1.4.7. 2-(6-Methoxy-3-pyridylamino)-3-isopropylimino-5-p-chlorophenyl-3,5-dihydrophenazine (7j). Yield: 45%; red solid; mp: 176–178 °C; ^1H NMR (500 MHz, CDCl_3) δ 8.15 (1H, d, J = 2.2 Hz, Ar–H), 7.73–7.68 (2H, m, Ar–H), 7.67–7.62 (2H, m, Ar–H), 7.32–7.27 (2H, m, Ar–H), 7.18–7.14 (1H, m, Ar–H), 7.13–7.08 (1H, m, Ar–H), 6.79 (1H, d, J = 8.7 Hz, Ar–H), 6.49 (1H, s, 1-H), 6.44 (1H, d, J = 8.1 Hz, Ar–H), 5.28 (1H, s, 4-H), 3.96 (3H, s, Me), 3.53–3.41 (1H, m, CHMe_2), 1.10 (6H, d, J = 6.2 Hz, CHMe_2); ^{13}C NMR (126 MHz, CDCl_3) δ 161.2, 151.0, 150.5, 146.0, 142.5, 136.1, 135.6 (2), 135.2, 134.8, 131.7 (2), 131.3, 130.4 (2), 130.1, 128.1, 127.1, 122.9, 113.8, 111.0, 98.0, 89.0, 53.7, 49.4, 23.6 (2); HRMS: calcd for $\text{C}_{27}\text{H}_{25}\text{ON}_5\text{Cl}$ $[\text{M}+\text{H}]^+$ 470.1742, found: 470.1741.

4.1.4.8. 2-p-Chlorobenzylamino-3-isopropylimino-5-p-chlorophenyl-3,5-dihydrophenazine (7k). Yield: 64%; red solid; mp: 176–178 °C; ^1H NMR (400 MHz, CDCl_3) δ 7.70–7.66 (2H, m, Ar–H), 7.63 (1H, dd, J = 7.9, 1.4 Hz, Ar–H), 7.32–7.26 (6H, m, Ar–H), 7.16–7.11 (1H, m, Ar–H), 7.10–7.04 (1H, m, Ar–H), 6.41 (1H, d, J = 8.2 Hz, Ar–H), 6.06 (1H, s, 1-H), 5.23 (1H, s, 4-H), 4.47 (2H, s, CH_2Ar), 3.48–3.39 (1H, m, CHMe_2), 1.05 (6H, d, J = 6.2 Hz, CHMe_2); ^{13}C NMR (101 MHz, CDCl_3) δ 151.1, 150.5, 147.9, 136.6, 136.3, 135.6, 135.5, 134.6, 132.9, 131.6 (2), 131.2, 130.5 (2), 128.8 (2), 128.5 (2), 127.8, 126.8, 122.7, 113.7, 96.5, 89.0, 49.3, 46.1, 23.6 (2); HRMS: calcd for $\text{C}_{28}\text{H}_{25}\text{N}_4\text{Cl}_2$ $[\text{M}+\text{H}]^+$ 487.1451, found: 487.1449.

4.1.4.9. 2-Benzylamino-3-isopropylimino-5-phenyl-3,5-dihydrophenazine (7p). Yield: 64%; red solid; mp: 199–201 °C; ^1H NMR (400 MHz, CDCl_3) δ 7.72–7.67 (2H, m, Ar–H), 7.66–7.59 (2H, m, Ar–H), 7.38–7.29 (7H, m, Ar–H), 7.16–7.10 (1H, m, Ar–H), 7.09–7.03 (1H, m, Ar–H), 6.44 (1H, d, J = 7.7 Hz, Ar–H), 6.14 (1H, s, 1-CH), 5.23 (1H, s, 4-CH), 4.50 (2H, s, CH_2Ar), 3.42–3.33 (1H, m, CHMe_2), 1.02 (6H, d, J = 6.2 Hz, CHMe_2); ^{13}C NMR (126 MHz, $\text{DMSO}-d_6$) δ 149.7, 145.3, 142.2, 138.5, 137.4, 136.0, 134.6, 131.1 (3), 130.8, 129.3, 128.9, 128.5 (2), 127.5 (2), 127.3 (2), 127.2, 127.1, 117.0, 100.3, 89.6, 46.2, 45.9, 20.6 (2); HRMS: calcd for $\text{C}_{28}\text{H}_{27}\text{N}_4$ $[\text{M}+\text{H}]^+$ 419.2230, found: 419.2231.

4.1.4.10. 2-p-Fluorobenzylamino-3-isopropylimino-5-phenyl-3,5-dihydrophenazine (7q). Yield: 61%; red solid; mp: 166–168 °C; ^1H NMR (500 MHz, CDCl_3) δ 7.73–7.68 (2H, m, Ar–H), 7.67–7.60 (2H, m, Ar–H), 7.34–7.29 (4H, m, Ar–H), 7.13 (1H, t, J = 7.3 Hz, Ar–H), 7.09–7.00 (3H, m, Ar–H), 6.45 (1H, d, J = 8.1 Hz, Ar–H), 6.10 (1H, s, 1-CH), 5.22 (1H, s, 4-CH), 4.47 (2H, s, CH_2Ar), 3.41–3.33 (1H, m, CHMe_2), 1.02 (6H, d, J = 6.3 Hz, CHMe_2); ^{13}C NMR (126 MHz, CDCl_3) δ 162.0 (d, J = 244.0 Hz, 1C–F), 151.1, 150.7, 147.9, 137.8, 135.6, 134.8, 133.8, 131.5, 131.2 (2), 129.6, 128.9 (2), 128.8, 128.7, 127.6, 126.7, 122.5, 115.5 (2) (d, J = 22.0 Hz, 2C–F), 114.0, 96.3, 89.1, 49.2, 46.0, 23.5 (2); HRMS: calcd for $\text{C}_{28}\text{H}_{26}\text{N}_4\text{F}$ $[\text{M}+\text{H}]^+$ 437.2136, found: 437.2136.

4.1.5. Synthesis of 2-*p*-fluoroanilino-3-isopropylimino-5-*p*-chlorophenyl-3,5-dihydrophenazine **15a**

To a solution of 2-fluoronitrobenzene (21.0 mmol) in DMF (35 mL), **8a** (1.1 equiv) and TEA (1.5 equiv) were added. The reaction mixture was warmed to 90 °C and stirred for 14 h the mixture was cooled to rt and partitioned between ethyl acetate (50 mL) and water (50 mL), and the water phase was extracted with ethyl acetate. The combined organic phases were washed with 2 N HCl (60 mL x 2) and brine (80 mL x 2), dried over anhydrous Na₂SO₄, filtered and evaporated. The residue recrystallized in ethanol to give **9a**. Yield: 61%; red solid; ¹H NMR (500 MHz, DMSO-*d*₆) δ 9.36 (1H, br s, NH), 8.12 (1H, dd, *J* = 8.5, 1.5 Hz, Ar-H), 7.53–7.46 (1H, m, Ar-H), 7.39–7.35 (2H, m, Ar-H), 7.30–7.24 (2H, m, Ar-H), 7.07–7.04 (1H, m, Ar-H), 6.89–6.84 (1H, m, Ar-H).

Intermediate **9a** (12.9 mmol) and 10% Pd/C (0.2 equiv) were suspended in ethanol (90 mL), and the mixture was shaken under hydrogen atmosphere for 6 h. The mixture was then filtered to achieve a solution of crude **10a** in ethanol. Following similar procedures in 4.1.2 and 4.1.4 subsequently, **2a** was replaced by **10a**, the compound **15a** was gained. Yield: 48%; red solid; mp: 180–182 °C; ¹H NMR (400 MHz, CDCl₃) δ 7.69 (1H, dd, *J* = 7.7, 1.4 Hz, Ar-H), 7.45–7.38 (2H, m, Ar-H), 7.35–7.27 (6H, m, Ar-H), 7.20–7.09 (2H, m, Ar-H), 6.83 (1H, s, 1-CH), 6.45 (1H, d, *J* = 8.1 Hz, Ar-H), 5.26 (1H, s, 4-CH), 3.49–3.39 (1H, m, CHMe₂), 1.08 (6H, d, *J* = 6.2 Hz, CHMe₂); ¹³C NMR (101 MHz, CDCl₃) δ 162.8, 151.1, 150.5, 143.7, 138.7, 135.7, 135.1, 133.5, 131.7, 130.9, 130.8, 129.3 (2), 128.2 (2), 127.5, 122.9, 122.8 (2), 118.6, 118.4, 113.9, 99.1, 89.1, 49.4, 23.6 (2); HRMS: calcd for C₂₇H₂₃N₄ClF [M+H]⁺ 457.1590, found: 457.1590.

4.1.6. Synthesis of 2-*p*-chloroanilino-3-isopropylimino-5-(6-methoxy-3-pyridinyl)-3,5-dihydrophenazine **15c**

To a solution of 2-fluoronitrobenzene (70.9 mmol) in DMF (70 mL), **8b** (1.0 equiv) and NaHCO₃ (1.2 equiv) were added. The reaction was stirred for 48 h at 100 °C before it was diluted with ethyl acetate (50 mL) and water (50 mL), and the water phase was extracted two times with ethyl acetate. The combined organic phases were washed with brine (100 mL x 2), dried over anhydrous Na₂SO₄, filtered and concentrated. The residue recrystallized in petroleum ether/ethanol to give **9b**. Yield: 55%; red solid; ¹H NMR (500 MHz, DMSO-*d*₆) δ 9.35 (1H, br s, NH), 8.16 (1H, d, *J* = 2.7 Hz, Ar-H), 8.12 (1H, dd, *J* = 8.5, 1.5 Hz, Ar-H), 7.70 (1H, dd, *J* = 8.7, 2.7 Hz, Ar-H), 7.49–7.45 (1H, m, Ar-H), 6.93–6.87 (2H, m, Ar-H), 6.85–6.81 (1H, m, Ar-H), 3.88 (3H, s, OMe).

Intermediate **9b** (12.9 mmol) and 10% Pd/C (0.2 equiv) were suspended in ethanol (90 mL), and the mixture was shaken under hydrogen atmosphere for 6 h. The mixture was then filtered to achieve a solution of **10b**, which was taken as starting material instead of **2a**, following similar procedures in 4.1.2 and 4.1.4 subsequently, to achieve **15c**. Yield: 55%; red solid; mp: 199–201 °C; ¹H NMR (400 MHz, CDCl₃) δ 8.17 (1H, d, *J* = 2.5 Hz, Ar-H), 7.68 (1H, dd, *J* = 7.7, 1.3 Hz, Ar-H), 7.57 (1H, dd, *J* = 8.7, 2.6 Hz, Ar-H), 7.34–7.28 (4H, m, Ar-H), 7.20–7.10 (2H, m, Ar-H), 7.08 (1H, d, *J* = 8.7 Hz, Ar-H), 6.83 (1H, s, 1-CH), 6.49 (1H, d, *J* = 7.8 Hz, Ar-H), 5.32 (1H, s, 4-CH), 4.09 (3H, s, OMe), 3.55–3.44 (1H, m, CHMe₂), 1.13–1.07 (6H, m, CHMe₂); ¹³C NMR (101 MHz, CDCl₃) δ 164.3, 151.2, 150.4, 147.6, 143.7, 139.4, 138.6, 135.7, 135.4, 132.0, 129.3 (2), 128.3, 128.2, 127.8, 127.6, 123.0, 122.9 (2), 113.8, 113.5, 99.1, 89.2, 54.2, 49.4, 23.7, 23.5; HRMS: calcd for C₂₇H₂₅ClN₅O [M+H]⁺ 470.1742, found: 470.1743.

4.1.7. General synthesis of compounds **15d–j**

Following a similar procedure in preparing **4a–h** in 4.1.2, the reaction of **10b** with corresponding intermediates **12c–g**. Then, the mixture of **12c–g** (1 g) and 10% Pd/C (0.2 equiv.) in methanol (30 mL) and THF (30 mL) was shaken overnight under hydrogen atmosphere. The reaction mixture was filtered, and the filtrate was

concentrated *in vacuo*. The residue suspended or dissolved in ethanol/CH₂Cl₂, and then stood still under air overnight. The precipitate was filtered, and then washed with ethanol to give compounds **14c–g** respectively, in total yields of 64–65%.

Following similar procedures in 4.1.4, the reaction of **14c–g** with amines achieved the title compounds **15d–j**.

4.1.7.1. 2-Anilino-3-isopropylimino-5-(6-methoxy-3-pyridinyl)-3,5-dihydrophenazine (**15d**). Yield: 50%; red solid; mp: 214–216 °C; ¹H NMR (500 MHz, CDCl₃) δ 11.03 (1H, s, NH), 8.29 (1H, s, Ar-H), 8.17 (1H, d, *J* = 8.2 Hz, Ar-H), 7.72 (1H, d, *J* = 7.0 Hz, Ar-H), 7.63 (1H, t, *J* = 7.6 Hz, Ar-H), 7.59–7.53 (4H, m, Ar-H), 7.45–7.39 (2H, m, Ar-H), 7.23–7.19 (2H, m, Ar-H), 7.02 (1H, d, *J* = 8.5 Hz, Ar-H), 5.87 (1H, s, 1-CH), 4.15 (3H, s, OMe), 3.75–3.66 (1H, m, CHMe₂), 1.50 (6H, d, *J* = 11.6 Hz, CHMe₂); ¹³C NMR (126 MHz, CDCl₃) δ 165.5, 152.2, 146.1, 145.3, 142.8, 138.6, 137.7, 137.2, 136.5, 130.8, 129.8, 129.6 (2), 129.0, 127.4, 126.3, 125.7, 123.9 (2), 116.2, 113.9, 102.5, 89.7, 54.7, 48.2, 21.2, 21.1; HRMS: calcd for C₂₇H₂₆ON₅ [M+H]⁺ 436.2132, found: 436.2131.

4.1.7.2. 2-*p*-Methoxyanilino-3-isopropylimino-5-(6-methoxy-3-pyridinyl)-3,5-dihydro phenazine (**15e**). Yield: 51%; red solid; mp: 164–166 °C; ¹H NMR (500 MHz, CDCl₃) δ 8.17 (1H, d, *J* = 2.3 Hz, Ar-H), 7.66 (1H, d, *J* = 7.7 Hz, Ar-H), 7.57 (1H, dd, *J* = 8.7, 2.5 Hz, Ar-H), 7.30–7.27 (2H, m, Ar-H), 7.16 (1H, t, *J* = 7.3 Hz, Ar-H), 7.11 (1H, d, *J* = 7.5 Hz, Ar-H), 7.08 (1H, d, *J* = 8.6 Hz, Ar-H), 6.94–6.89 (2H, m, Ar-H), 6.66 (1H, s, 1-CH), 6.48 (1H, d, *J* = 8.1 Hz, Ar-H), 5.32 (1H, s, 4-CH), 4.09 (3H, s, OMe), 3.83 (3H, s, OMe), 3.54–3.48 (1H, m, CHMe₂), 1.10 (6H, dd, *J* = 10.2, 6.3 Hz, CHMe₂); ¹³C NMR (126 MHz, CDCl₃) δ 164.2, 156.4, 151.3, 150.5, 147.6, 145.5, 139.5, 135.8, 135.3, 132.7, 131.8, 128.0, 127.9, 127.0, 124.5 (2), 122.8, 114.5 (2), 113.7, 113.4, 97.6, 89.1, 55.6, 54.1, 49.4, 23.7, 23.6; HRMS: calcd for C₂₈H₂₈N₅O₂ [M + H]⁺ 466.2238, found: 466.2238.

4.1.7.3. 2-*m*-Fluoroanilino-3-isopropylimino-5-(6-methoxy-3-pyridinyl)-3,5-dihydro phenazine (**15f**) Yield: 57%; red solid; mp: 209–211 °C; ¹H NMR (400 MHz, CDCl₃) δ 8.17 (1H, d, *J* = 2.6 Hz, Ar-H), 7.70 (1H, dd, *J* = 7.7, 1.6 Hz, Ar-H), 7.57 (1H, dd, *J* = 8.7, 2.7 Hz, Ar-H), 7.34–7.27 (1H, m, Ar-H), 7.20–7.07 (5H, m, Ar-H), 6.92 (1H, s, 1-CH), 6.80–6.74 (1H, m, Ar-H), 6.49 (1H, d, *J* = 8.0 Hz, Ar-H), 5.33 (1H, s, 4-CH), 4.09 (3H, s, OMe), 3.56–3.45 (1H, m, CHMe₂), 1.12–1.08 (6H, m, CHMe₂); ¹³C NMR (101 MHz, CDCl₃) δ 164.3 (d, *J* = 244.0 Hz, 1C-F), 163.4, 151.2, 150.3, 147.6, 143.3, 141.8, 139.5, 135.7, 135.4, 132.0, 130.0, 128.3, 127.8, 127.7, 123.0, 116.9, 113.8, 113.5, 109.9 (d, *J* = 21.0 Hz, 2C-F), 108.3 (d, *J* = 24.0 Hz, 2CF), 99.8, 89.2, 54.2, 49.4, 23.7, 23.5; HRMS: calcd for C₂₇H₂₅FN₅O [M+H]⁺ 454.2038, found: 454.2040.

4.1.7.4. 2-*p*-Fluoroanilino-3-isopropylimino-5-(6-methoxy-3-pyridinyl)-3,5-dihydro phenazine (**15g**). Yield: 55%; red solid; mp: 210–212 °C; ¹H NMR (500 MHz, CDCl₃) δ 8.17 (1H, d, *J* = 2.6 Hz, Ar-H), 7.67 (1H, dd, *J* = 7.8, 1.4 Hz, Ar-H), 7.57 (1H, dd, *J* = 8.7, 2.6 Hz, Ar-H), 7.34–7.29 (2H, m, Ar-H), 7.18–7.05 (5H, m, Ar-H), 6.71 (1H, s, 1-CH), 6.49 (1H, d, *J* = 8.1 Hz, Ar-H), 5.33 (1H, s, 4-CH), 4.09 (3H, s, OMe), 3.56–3.47 (1H, m, CHMe₂), 1.10 (6H, dd, *J* = 10.3, 6.3 Hz, CHMe₂); ¹³C NMR (126 MHz, CDCl₃) δ 164.3, 159.2 (d, *J* = 244.4 Hz, 1C-F), 151.2, 150.4, 147.6, 144.8, 139.5, 135.9, 135.7, 135.3, 131.9, 128.2, 127.8, 127.4, 124.2 (2), 122.9, 116.0 (2) (d, *J* = 22.5 Hz, 2C-F), 113.8, 113.4, 98.2, 89.1, 54.2, 49.4, 23.7, 23.5; HRMS: calcd for C₂₇H₂₅FN₅O [M+H]⁺ 454.2038, found: 454.2036.

4.1.7.5. 2-*p*-Fluoroanilino-3-cyclopropylimino-5-(6-methoxy-3-pyridinyl)-3,5-dihydro phenazine (**15h**). Yield: 57%; red solid; mp: 211–213 °C; ¹H NMR (400 MHz, CDCl₃) δ 8.18 (1H, d, *J* = 2.5 Hz, Ar-H), 7.65 (1H, dd, *J* = 7.7, 1.5 Hz, Ar-H), 7.59 (1H, dd, *J* = 8.7,

2.7 Hz, Ar-H), 7.30–7.26 (2H, m, Ar-H), 7.18–7.10 (2H, m, Ar-H), 7.09–7.03 (3H, m, Ar-H), 6.65 (1H, s, 1-CH), 6.47 (1H, d, $J = 8.0$ Hz, Ar-H), 5.59 (1H, s, 4-CH), 4.08 (3H, s, OMe), 2.82–2.75 (1H, m, CHCH₂CH₂), 0.93–0.87 (2H, m, CHCH₂CH₂), 0.82–0.78 (2H, m, CHCH₂CH₂); ¹³C NMR (101 MHz, CDCl₃) δ 164.3, 159.3 (d, $J = 244.4$ Hz, 1C-F), 152.5, 151.4, 147.7, 144.7, 139.6, 135.8 (2), 135.1, 132.0, 128.1, 127.8, 127.4, 124.5, 124.4, 122.9, 116.2 (2) (d, $J = 27.5$ Hz, 2C-F), 113.7, 113.5, 98.2, 89.6, 54.1, 33.0, 10.0 (2); HRMS: calcd for C₂₇H₂₃FN₅O [M+H]⁺ 452.1881, found: 452.1881.

4.1.7.6. 2-p-Fluoroanilino-3-propylimino-5-(6-methoxy-3-pyridinyl)-3,5-dihydro phenazine (15i). Yield: 49%; red solid; mp: 186–188 °C; ¹H NMR (400 MHz, CDCl₃) δ 8.17 (1H, d, $J = 2.3$ Hz, Ar-H), 7.69 (1H, d, $J = 6.7$ Hz, Ar-H), 7.57 (1H, dd, $J = 8.7, 2.6$ Hz, Ar-H), 7.35–7.28 (2H, m, Ar-H), 7.22–7.12 (2H, m, Ar-H), 7.11–7.04 (3H, m, Ar-H), 6.72 (1H, s, 1-CH), 6.51 (1H, d, $J = 7.0$ Hz, Ar-H), 5.31 (1H, s, 4-CH), 4.09 (3H, s, OMe), 3.14 (2H, t, $J = 5.8$ Hz, CH₂CH₂CH₃) 1.73–1.65 (2H, m, CH₂CH₂CH₃), 0.95 (3H, t, $J = 7.4$ Hz, CH₂CH₂CH₃); ¹³C NMR (101 MHz, CDCl₃) δ 164.3, 159.3 (d, $J = 244.4$ Hz, 1C-F), 152.4, 151.2, 147.5, 144.7, 139.4, 135.8 (2), 135.3, 131.8, 128.2, 127.8, 127.5, 124.3 (2) (d, $J = 8.0$ Hz, 3C-F), 123.1, 116.1 (2) (d, $J = 25.0$ Hz, 2C-F), 113.9, 113.5, 98.2, 89.2, 54.2, 52.0, 24.3, 12.3; HRMS: calcd for C₂₇H₂₅FN₅O [M+H]⁺ 454.2038, found: 454.2035.

4.1.7.7. 2-p-Fluoroanilino-3-(4-methoxycyclohexylimino)-5-(6-methoxy-3-pyridinyl)-3,5-dihydrophenazine (15j). Yield: 54%; orange solid; mp: 176–178 °C; ¹H NMR (400 MHz, CDCl₃) δ 8.16 (1H, d, $J = 2.4$ Hz, Ar-H), 7.70–7.65 (1H, m, Ar-H), 7.56 (1H, dd, $J = 8.7, 2.6$ Hz, Ar-H), 7.33–7.28 (2H, m, Ar-H), 7.20–7.11 (2H, m, Ar-H), 7.10–7.04 (3H, m, Ar-H), 6.72 (1H, s, 1-H), 6.53 (1H, d, $J = 7.5$ Hz, Ar-H), 5.29 (1H, s, 4-H), 4.08 (3H, s, OMe), 3.36 (3H, s, OMe), 3.24–3.10 (2H, m, N-CH, O-CH), 2.12–2.03 (2H, m, CH₂), 1.76–1.66 (2H, m, CH₂), 1.47–1.37 (2H, m, CH₂), 1.24–1.14 (2H, m, CH₂); ¹³C NMR (101 MHz, CDCl₃) δ 164.4, 159.3 (d, $J = 242.0$ Hz, 1C-F), 151.2, 151.1, 147.5, 144.7, 139.3, 135.8, 135.7, 135.3, 131.8, 128.2, 127.7, 127.5, 124.2 (2), 123.0, 116.2 (2) (d, $J = 22.0$ Hz, 2C-F), 113.8, 113.3, 98.3, 89.1, 57.3, 55.9, 54.2, 31.2, 31.2, 30.0 (2); HRMS: calcd for C₃₁H₃₁FN₅O₂ [M+H]⁺ 524.2456, found: 524.2456.

4.2. Biology

4.2.1. Cell lines, plasmids, and viruses

BSR and 293T cells were cultured in 5% CO₂ at 37 °C in high glucose Dulbecco's Modified Eagle's Medium (HyClone, South Logan, UT) supplemented with 10% FBS (Gibco, Carlsbad, CA), and 1% penicillin–streptomycin solution (Gibco, Carlsbad, CA). Cells were passaged every 2 days. Virulent rabies virus CVS strain was adapted by BSR (variant strain of BHK) cells, and stored at –70 °C. The pSARS-Cov-2 virus was constructed as described previously [20].

4.2.2. Anti-rabies activity evaluation

Following a similar RFFIT method as described previously [9], serial dilutions of test compounds, starting from 200 μ M were incubated with 50 μ L of CVS (20,000 FFU/well) in duplicate at 37 °C for 1 h, then mixed with BSR cells (1×10^6 /ml) and subsequently incubated for 24 h. Then, after being fixed with pre-chilled 80% acetone, the cells were stained with fluorescein isothiocyanate (FITC)-conjugated anti-rabies N monoclonal antibody (Fujirebio Diagnostics, Malvern, PA), and the fluorescent intensity was recorded by a fluorescence microscope (Olympus, Tokyo, Japan). The EC₅₀ value was determined from the dose-response curve.

4.2.3. Anti-pSARS-CoV-2 activity evaluation

Following a similar method as described previously [20,21], serial dilutions of test compounds, starting from 200 μ M were incubated with 1.3×10^4 TCID₅₀ of pSARS-CoV-2 at 37 °C for 1 h, then mixed with Huh 7 cells (2000 cells/well) and subsequently incubated for 24 h. The bioluminescence intensities were recorded to calculate EC₅₀ value of each compound as described previously [20].

4.2.4. Cytotoxicity testing

Serial dilutions of test compounds, starting from 200 μ M were incubated with BSR cells or 293T cells in 96-well plates, then 50 μ L of medium was added instead of virus. After being incubated at 37 °C for 24 h, the cell viability was recorded by an Ensignt microplate luminometer (PerkinElmer, Singapore), and the CC₅₀ values of test compounds were calculate by GraphPad Prism 6 (San Diego, CA).

4.2.5. Acute toxicity

Female Kunming mice with weight of 20.0 ± 1.0 g were obtained from the Institute of Laboratory Animal Science (Beijing, China). The experiment was performed in accordance with the guidelines established by the Institute of Medicinal Biotechnology, Peking Union Medical College and Chinese Academy of Medical Science for the care and use of laboratory animals. The mice were fed with regular rodent chow and housed in an air-conditioned room. The mice were randomly divided into different groups with 6 mice each. Each compound was given orally in a single-dosing experiment at 0, 200, 400, 600 or 800 mg•kg⁻¹ (ddH₂O as control), respectively. The mice were closely monitored for 7 days. Body weight, behavior change and survival were monitored.

4.2.6. Time of addition assay

The “time-of-addition” experiment was performed as described previously [9]. Specifically, compounds **15f** and **15g** were applied as the test compound, and **1** was used as positive control. Data were analyzed based on three replicates.

4.2.7. Molecular modeling analysis

The protein crystal structures were obtained from the RCSB Protein Data Bank (<https://www.rcsb.org>). Discovery Studio 4.5 software (BIOVIA, San Diego, California, USA) was applied for both ligand and protein preparation using the default settings. Libdock program was employed and Libdock score function was applied to evaluate the affinity of the receptor-ligand interaction. The docking conformation with the highest score was chosen to inspect the binding modes.

4.2.8. SPR

Rabies virus G protein (20–459 AA residues) with a GST-His tag was cloned into pET28a vector and grown in E. coli BL21 (DE3) cells. The bacteria were grown at 37 °C until the OD₆₀₀ value of the liquid reaches 0.6–0.8 following induction with 0.5 mM isopropyl- β -D-thiogalactopyranoside (IPTG). The protein was then purified using the Ni²⁺-loaded HiTrap Chelating System (GE Healthcare, US) according to the manufacturer's instructions. SARS-CoV-2 S recombinant protein was purchased from Sino biological Inc (Beijing, China). The S series CM5 sensor chip and amine coupling Kit were purchased from GE Healthcare (Uppsala, Sweden). The PBS-P buffer was filtered through a 0.45 μ m membrane filter and degassed before use. SPR analysis was performed on a Biacore™ T200 system (GE Healthcare, US) and PBS-P buffer was used as sample and running buffer. The target G or S protein was covalently immobilized into the CM5 sensor chip using an amine coupling kit in a sodium acetate solution of pH 4.0. Compounds **15f** and **1** were

diluted in a series of concentrations in PBS-P buffer, and flowed through the fixed protein at a rate of 30 $\mu\text{L}/\text{min}$, with a contact time of 60 s and a dissociation time of 120 s. Data were processed by subtracting responses from the reference flow cell and from the blank cycles. All data were analyzed by the kinetic model in the Biacore™ T200 Evaluation Software 2.0 (GE Healthcare, US), and Kd was applied to evaluate the binding affinity.

Declaration of competing interest

The authors declare that they have no known competing financial interests or personal relationships that could have appeared to influence the work reported in this paper.

Acknowledgements

This work was supported by the CAMS Innovation Fund for Medical Sciences (2021–12M-1-048) and National Natural Science Foundation of China (81872912).

Appendix A. Supplementary data

Supplementary data to this article can be found online at <https://doi.org/10.1016/j.ejmech.2022.114209>.

References

- [1] M.J. Schnell, J.P. McGettigan, C. Wirblich, A. Papaneri, The cell biology of rabies virus: using stealth to reach the brain, *Nat. Rev. Microbiol.* 8 (2010) 51–61.
- [2] Z. Mi, L. Zhao, M. Sun, T. Gao, Y. Wang, B. Sui, Y. Li, Overexpression of interleukin-33 in recombinant rabies virus enhances innate and humoral immune responses through activation of dendritic cell-germinal center reactions, *Vaccines (Basel)* 10 (2021) 34.
- [3] WHO/Department of control of neglected tropical diseases, WHO expert consultation on rabies. Third report, World Health Organ, Tech. Rep. (2018) 1–141, back cover.
- [4] D. Wentworth, K. Hampson, S.M. Thumbi, A. Mwatondo, G. Wambura, N.R. Chng, A social justice perspective on access to human rabies vaccines, *Vaccine* 37 (Suppl 1) (2019) A3–A5.
- [5] A. Gholami, M.R. Shirzadi, M. Asouri, F. Farahtaj, E. Mostafavi, S. Gharibzadeh, J. Pourmozafari, M. Nabavi, F. Nazari, F. Bahrami, Seroconversion after three doses of intramuscular rabies vaccine as a post-exposure treatment, *Virus Res.* 278 (2020) 197883.
- [6] C.H. Tran, D.O. Afriyie, T.N. Pham, S. Otsu, M. Urabe, A.D. Dang, H.G.T. Tran, H.V. Nguyen, H.T. Le, H.T.T. Nguyen, Rabies post-exposure prophylaxis initiation and adherence among patients in Vietnam, 2014–2016, *Vaccine* 37 (Suppl 1) (2019) A54–A63.
- [7] A.C. Jackson, Update on rabies diagnosis and treatment, *Curr. Infect. Dis. Rep.* 11 (2019) 296–301.
- [8] G. Daniel, A. Julia, Overview, prevention, and treatment of rabies, *Mayo Clin. Proc.* 79 (2004) 671–676.
- [9] J. Wu, S. Cao, S. Lei, Q. Liu, Y. Li, Y. Yu, H. Xie, Q. Li, X. Zhao, R. Chen, W. Huang, X. Xiao, Y. Yu, D. Song, Y. Li, Y. Wang, Clofazimine: a promising inhibitor of rabies virus, *Front. Pharmacol.* 12 (2021) 598241.
- [10] S. Yuan, X. Yin, X. Meng, J.F. Chan, Z.W. Ye, L. Riva, L. Pache, C.C. Chan, P.M. Lai, C.C. Chan, V.K. Poon, A.C. Lee, N. Matsunaga, Y. Pu, C.K. Yuen, J. Cao, R. Liang, K. Tang, L. Sheng, Y. Du, W. Xu, C.Y. Lau, K.Y. Sit, W.K. Au, R. Wang, Y.Y. Zhang, Y.D. Tang, T.M. Clausen, J. Pihl, J. Oh, K.H. Sze, A.J. Zhang, H. Chu H, K.H. Kok, D. Wang D, X.H. Cai, J.D. Esko, I.F. Hung, R.A. Li, H. Chen, H. Sun, D.Y. Jin, R. Sun, S.K. Chanda, K.Y. Yuen, Clofazimine broadly inhibits coronaviruses including SARS-CoV-2, *Nature* 593 (2021) 418–423.
- [11] M.D. Murashov, V. LaLone, P.M. Rzeczycki, R.K. Keswani, G.S. Yoon, S. Sud, W. Rajeswaran, S. Larsen, K.A. Stringer, G.R. Rosania, The physicochemical basis of clofazimine-induced skin pigmentation, *J. Invest. Dermatol.* 138 (2018) 697–703.
- [12] A. Koval, I. Bassanini, J. Xu, M. Tonelli, V. Boido, F. Sparatore, F. Amant, D. Annibali, E. Leucci, A. Sparatore, V.L. Katanaev, Optimization of the clofazimine structure leads to a highly water-soluble C3-aminopyridinyl riminophenazine endowed with improved anti-Wnt and anti-cancer activity in vitro and in vivo, *Eur. J. Med. Chem.* 222 (2021) 113562.
- [13] D. Zhang, Y. Lu, K. Liu, B. Liu, J. Wang, G. Zhang, H. Zhang, Y. Liu, B. Wang, M. Zheng, L. Fu, Y. Hou, N. Gong, Y. Lv, C. Li, C.B. Cooper, A.M. Upton, D. Yin, Z. Ma, H. Huang, Identification of less lipophilic riminophenazine derivatives for the treatment of drug-resistant tuberculosis, *J. Med. Chem.* 55 (2012) 8409–8417.
- [14] I. Bassanini, S. Parapini, N. Basilico, A. Sparatore, Novel hydrophilic riminophenazines as potent antiprotozoal agents, *ChemMedChem* 14 (2019) 1940–1949.
- [15] H. Rubin, T. Yano, S. Kassovska-Bratinova, N. Schechter, J.S. Teh, J. Winkler, Novel Therapeutic Agents, U.S. Pat. Appl. Publ., 2014. US 20140371228 A1.
- [16] C.E. Medlen, R. Anderson, J.F.G. O'Sullivan, Use of a riminophenazine for treating MDR resistance, *Eur. Pat. Appl.* (1995). EP 676201 A2.
- [17] K. Liu, C.B. Cooper, H. Huang, C. Li, B. Liu, Y. Liu, Z. Ma, J. Wang, D. Yin, D. Zhang, G. Zhang, H. Zhang, Riminophenazines with 2-(heteroaryl)amino substituents and their anti-microbial activity, *PCT Int. Appl.* (2012). WO 2012003190 A1.
- [18] J.E. Savage, J.F. O'Sullivan, B.M. Zeis, R. Anderson, Investigation of the structural properties of dihydrophenazines which contribute to their pro-oxidative interactions with human phagocytes, *J. Antimicrob. Chemother.* 23 (1989) 691–700.
- [19] Y. Wang, H. Xie, Q. Liu, S. Cao, W. Huang, J. Nie, C. Zhao, Application of Imino Phenazines as Rabies Virus Inhibitors, Faming Zhuanli Shenqing, 2018. CN 108853106A.
- [20] J. Nie, Q. Li, J. Wu, C. Zhao, H. Hao, H. Liu, L. Zhang, L. Nie, H. Qin, M. Wang, Q. Lu, X. Li, Q. Sun, J. Liu, C. Fan, W. Huang, M. Xu, Y. Wang, Establishment and validation of a pseudovirus neutralization assay for SARS-CoV-2, *Emerg. Microb. Infect.* 9 (2020) 680–686.
- [21] K. Wang, J.J. Wu, X. Zhang, Q.X. Zeng, N. Zhang, W.J. Huang, S. Tang, Y.X. Wang, W.J. Kong, Y.C. Wang, Y.H. Li, D.Q. Song, Discovery and evolution of 12N-substituted aloperine derivatives as anti-SARS-CoV-2 agents through targeting late entry stage, *Bioorg. Chem.* 115 (2021) 105196.
- [22] F. Zandi, F. Goshadrrou, A. Meyfour, B. Vaziri, Rabies infection: an overview of lyssavirus-host protein interactions, *Iran. Biomed. J.* 25 (2021) 226–242.